Extinction Coefficient of Gold Nanostars

The Extinction Coefficient of Gold Nanostars

Journal:	*The Journal of Physical Chemistry*
Manuscript ID:	jp-2015-03624p.R1
Manuscript Type:	Article
Date Submitted by the Author:	n/a
Complete List of Authors:	de Puig, Helena; Massachusetts Institute of Technology, Mechanical Engineering Tam, Justina; Massachusetts Institute of Technology, Institute for Medical Engineering and Science Yen, Chun-Wan; Georgia Institute of Technology, Chemistry and Biochemistry Gehrke, Lee; Massachusetts Institute of Technology, Institute for Medical Engineering and Science Hamad-Schifferli, Kimberly; Massachusetts Institute of Technology, Mechanical Engineering

The Extinction Coefficient of Gold Nanostars

Helena de Puig[1], Justina O. Tam[2,3], Chun-Wan Yen[2,3]†, Lee Gehrke[2,4], Kimberly Hamad-Schifferli[1]*‡*

[1]Dept. of Mechanical Engineering, Massachusetts Institute of Technology, Cambridge, MA 02139

[2]Institute for Medical Engineering and Science, Massachusetts Institute of Technology Cambridge, MA USA 02139

[3]Winchester Engineering Analytical Center, Food and Drug Administration. Winchester MA USA 01890

[4]Dept. of Microbiology and Immunobiology, Harvard Medical School, Boston 02115

ABSTRACT

Gold nanostars (NStars) are highly attractive for biological applications due to their surface chemistry, facile synthesis and optical properties. Here, we synthesize NStars in HEPES buffer at different HEPES/Au ratios, producing NStars of different sizes and shapes, and therefore varying

optical properties. We measure the extinction coefficient of the synthesized NStars at their maximum surface plasmon resonances (SPR), which range from 5.7 x 10^8 to 26.8 x 10^8 $M^{-1}cm^{-1}$. Measured values correlate with those obtained from theoretical models of the NStars using the discrete dipole approximation (DDA), which we use to simulate the extinction spectra of the nanostars. Finally, because NStars are typically used in biological applications, we conjugate DNA and antibodies to the NStars and calculate the footprint of the bound biomolecules.

KEYWORDS

Gold nanostar, molar extinction coefficient, HEPES, multibranched gold nanoparticle, nanoflower, optical properties, DDSCAT, DDA, discrete dipole approximation.

INTRODUCTION

Gold nanoparticles (Au NPs) are attractive for interacting with biological systems due to their small dimensions, surface chemistry and optical properties. They can be synthesized in a variety of sizes and shapes, resulting in different chemical and physical properties. Au nanostars (NStars), highly branched gold nanocrystals[1] or nanoflowers[2], are of particular interest because minor shape modifications enable manipulation of their optical properties. They possess a surface plasmon resonance (SPR) peak that is tunable throughout the visible and near IR spectrum, resulting in different extinction profiles and therefore distinct colors [3-5]. Due to their sharp tips, NStars have a narrow SPR, facilitating selective excitation with a laser and enabling optical absorption tunability.[1, 6, 7] Furthermore, their synthesis is facile and can be done in an aqueous nontoxic buffer[1], making NStars amenable for biological applications in targeted photothermal therapy and theranostics[4, 8, 9], imaging[10], sensors[11], and Surface Enhanced Raman Spectroscopy (SERS)[2, 6, 9, 12]. Because of the increasing interest in the optical and physical

properties of NStars, a variety of synthesis approaches have been developed using different surfactants and reducing agents[6, 7, 13, 14], which can yield to the formation of NStars of different symmetries. Nevertheless, many applications of nanostars are complicated by the lack of a simple manner to quantify their concentration. Au NStars absorb strongly in the visible spectrum. Their molar extinction coefficient, ε, is a fundamental parameter that allows for quantifying their concentration, and is thus critical for characterizing their behavior in therapeutic and sensing applications. ε is also essential for bioconjugation, as it allows for quantification of the biomolecule surface density and footprint on the NStars. Most importantly, understanding the relationship between ε and the NStar size/shape opens new avenues for the design of NStars with desired optical properties for particular applications, such as SERS[15], two photon luminescence[5], surface enhanced fluorescence, or localized surface plasmon resonance spectroscopy[11].

For spherical Au NPs and Au nanorods (NRs), ε has been widely studied and characterized[14, 16], and its dependence on nanoparticle physical dimensions is currently well understood. ε of nanospheres can be explicitly described as a function of nanosphere diameter, and thus can be calculated based on particle geometry. For NRs, both their SPR position and ε can be written as a function of their volume and aspect ratio. Agreement between experimental and computational models is generally very good. One model that has been widely used is the discrete dipole approximation (DDA), which relies on approximating a NP volume as an array of point dipoles, and calculates the interaction of electromagnetic radiation with the dipoles. This allows prediction of the extinction, absorption and scattering of light by metallic NPs of arbitrary shapes. In particular, the Fortran code DDSCAT has gained increasing interest as a reliable tool for modeling the optical properties of gold NPs. However, differences between computational

and experimental observations arise due to the variability in NP dimensions and shapes in solution, as well as interactions between NPs, which might not be accounted for in the computational model. [1, 14, 16, 17]

Here we present results quantifying ε as a function of size and shape for gold NStars, comparing experimental and computational measurements. First, we synthesize NStars of different sizes and shapes, which result in different SPRs. We experimentally quantify the ε of the different NStars and compare their values to those obtained by simulations by DDA. We observe that ε correlates with the NStar volume and SPR position, and similar trends are observed both experimentally and numerically. Finally, because of the growing interest of NStars for biological applications, we conjugate antibodies (Abs) and ssDNA aptamers onto the NStars, and use the experimentally measured ε values to quantify Ab and DNA surface coverage and footprint on the NStar surface. We observe that DNA surface coverage and footprint results agree with the measurements obtained for other well-established NPs, such as NRs and nanospheres. Ab coverage is lower in comparison, which could be attributed to a shape effect. This simple method for determining nanostar concentration has the potential to facilitate the use of Au NStars in biological and chemical applications.

EXPERIMENTAL METHODS

Reagents: Au chloride trihydrate was purchased from Sigma-Aldrich (CAS: 16961-25-4). Bis(sulphatophenyl)phenyl-phosphine dehydrate (BPS), was purchased from Aldrich (CAS:308103-66-4). N-(2-Hydroxyethyl)piperazine-N'-(2-ethanesulphonic acid) (HEPES) was purchased from United States Biochemical Company (CAT: 16926), sodium periodate (CAS: 7790-28-5) was purchased from Sigma, dithiolalkanearomatic PEG6-$NHNH_2$ (CAS: 963115-54-

7) was purchased from Sensopath Technologies. Tris(2-carboxyethyl)phosphine hydrochloride (TCEP) was purchased from Sigma. Gold standard for ICP was purchased from Fluka (38168-100 ml). Fluorescent Goat anti-Mouse IgG (H+L) Secondary Antibody, DyLight 650 conjugate was purchased from Pierce. Fluorescent ssDNA thrombin binding aptamer (TBA) with the sequence 5'/5ThioMC6-D/-(T_{15})-GGTTGGTGTGGTTGG-/36TAMSp/ 3' was purchased from IDT Technologies.

Synthesis of Au NStars: Au NStars with different extinction spectra were synthesized by tuning the Au/HEPES ratio in solution[1,3]. We tuned the concentration of HEPES from 28-140 mM, while keeping the Au concentration in solution constant. We mixed 200, 350, 500, 750 or 1000 µl of 140 mM HEPES with 800, 650, 500, 250 or 0 µl of 18 MΩ deionized water, followed by the addition of 16 µl of 25 mM $HAuCl_4 \cdot 3H_2O$ and further vortexing for the synthesis of NStar200, NStar350, NStar500, NStar750 and NStar1000, respectively. After vortexing, solutions sat undisturbed for 1 h, during which the NStars crystallized. Afterwards, ~ 0.5mg BPS was added for NStar stabilization, and the solution was vortexed and left undisturbed for 1 h. After this time, the NStars were ready to use in experiments. The NStars were separated from excess reagents by centrifugation at 10000 rcf for 15 min. The resulting NStar pellet was resuspended in 1 ml of 18 MΩ water.

Characterization of the NStars: Optical characterization of the NStars was performed with a Cary 100 UV Vis from Agilent Technologies. Morphology of the NStars was characterized with a FEI Tecnai G2 TEM at 120 kV, equipped with a single-tilt support that was used to tilt the samples ± 30º in order to observe their three-dimensional structure. ImageJ was used to process the images and measure the dimensions of the NStars.

Au ion concentrations were measured with the Activa-S ICP-AES from Horiba Jobin Yvon. 2 ml of the NStars were separated from unreacted gold in the solution by centrifugation at 10000 rcf, and resuspended in 1 ml of 18 MΩ deionized water. 150 µl of the purified Au nanoparticles were dissolved in 0.5 ml of aqua regia overnight, after which time they were diluted to 5 ml to produce a final concentration of 2% nitric acid. Au standards of 0, 2, 5, 10, and 20 ppm were prepared by diluting the 1 mg/ml Au standard from Fluka with 2 % nitric acid.

Ferguson Analysis and light scattering were used to calculate the hydrodynamic diameter and zeta potential (ζ) of gold NStars which has been previously described by others[18]. For the Ferguson analysis, gels of 0.5, 1, 1.5, 2 and 4 % agarose were run at 12 Vcm^{-1}, and the mobility of the nanoparticles was measured with ImageJ. NPs were loaded by mixing 8 µl of concentrated NStars with 4 µl of 50 % glycerol in 18 MΩ water. Spherical gold NPs synthesized by citrate reduction were used as standards to calculate the hydrodynamic diameter of the gold NStars and their ζ. In addition, a Zetasizer Nano ZS from Malvern Instruments was used to measure the hydrodynamic diameter (D_H) and the ζ of the Au NStars.

Theoretical Methods: DDA method with the DDSCAT package,[19] freely available in NanoHub.org- by Draine and Flatau was used to simulate the NStar optical response. In short, TEM images of NStars were analyzed with ImageJ to obtain average dimensions of every NP synthesis. These values were used to create 3D models of the NStars in AutoCAD (Autodesk), and area and volume of the particles were calculated. The 3D models were meshed using Blender and exported as .obj files (Scheme in Supporting Information, Figure SI-1). After, DDSCAT Convert, from Draine and Flatau was used to convert the .obj file into a collection of dipoles, which were used as input by DDSCAT to simulate the optical properties of the NStars. The

medium surrounding the NStars was considered to be water with a refractive index of 1.33. Au dielectric values were obtained from Johnson and Christy[20].

Bioconjugation of the NStars: Abs were covalently bound to Au NStars by directional conjugation[21]. In short, monoclonal Abs were attached to a heterobifunctional linker (dithiolalkanearomatic PEG6-NHNH27) consisting of a polyethylene chain with a hydrazide termination in one end and a dithiol in the other end. First, the hydroxyl moieties of the Fc region of the Abs were oxidized by mixing 50 µl of monoclonal Ab at 1 mg/ml in 40 mM HEPES, pH 7.4 with 5 µl of 10 mM $NaIO_4$ (Sigma). The solution was covered in foil and agitated for 45 min at room temperature. Then, 2 µl of a solution of 33 µg/ml heterobifunctional linker in ethanol and 250 µl of 1x PBS were added in the solution, and agitated for 30 min to allow binding of the linker to the Abs. Abs were concentrated using a 10 kDa centrifuge filter and diluted in 1X PBS to a final concentration of 1 mg/ml. To conjugate Abs to the NStars, 5 µl of the functionalized Abs were mixed with 1 ml of 2 nM NStars in 40 mM HEPES, at pH 7.4. The solution was continuously mixed for 30 min at room temperature during which time the Abs were able to bind to the nanoparticles. To remove unreacted Abs, the NStars were centrifuged for 10 min at 10000 rcf. Fluorescence spectroscopy was used to quantify the concentration of unbound Abs in the supernatant, which allowed calculation of the concentration of Ab bound to the NStars.

Single-stranded DNA (ssDNA) aptamers were covalently bound to the Au NStars by Au -thiol covalent conjugation. In short, dithiol bonds in the terminal 5' dithiol modifier of the ssDNA were reduced by mixing 5 µl of 100 mM TCEP at 4 ºC with 5 µl of 100 µM ssDNA. The solution sat undisturbed for 1h. In the meantime, a 20 µl pellet of NStars was prepared by centrifuging 1 ml of as prepared BPS-NStars at 10000 rcf for 15 min. The 20 µl NStar pellet was resuspended in 100 µl of 0.5x TBE and 4 µl of reduced ssDNA, vortexed and then concentrated by water

evaporation in a Savant SpeedVac at room temperature for 4 h, when 20-30 µl of solution were remaining in the tubes. After concentration, samples were sonicated at room temperature in a water bath and left undisturbed overnight. To separate bound and unbound DNA, 5 µl of the NStar pellets were diluted in 195 µl of water and centrifuged at 14000 rcf for 30 min. The supernatant, which contained the unbound DNA, was collected and fluorescence spectroscopy was used to quantify the bound ssDNA on the Au NStars.

RESULTS AND DISCUSSION

Synthesis and characterization of NStars

Au salts can be reduced in certain Good's buffers to form NStars. HEPES, in particular, is able to act as both a Au reducing agent and growth directing agent. HEPES reduces the Au^{3+} ions into Au^{0} [22], leading to the formation of gold NStars. The piperazine moiety of HEPES is thought to be responsible for the anisotropic growth of NStars[1]. We modified the HEPES reduction approach to tune the SPR across a broad wavelength range by varying the Au/HEPES ratio, a strategy that has been utilized in other NStar syntheses.[3] Tuning the Au/HEPES ratio changes the shape of the produced NStars, and thus results in NStars with different extinction spectra (see Methods for individual NStar synthesis procedures). This produced suspensions with colors that ranged from magenta to blue to green (Fig. 1a). Hydrodynamic diameter, D_H (Fig. 1b) and zeta potential (ζ) (Figure 1c, and Supporting Information Figure SI-2) of the NStars were measured by both dynamic light scattering (DLS, distribution in Supporting Information, Figure SI-3) and Ferguson analysis, and indicated similar characteristics between different preparations of the nanoparticles. Gel electrophoresis of the synthesized NStars showed that the NPs did not aggregate or smear when running in the gels (Figure 1d) indicating that BPS-coated NPs were

negatively charged and not aggregated. The different NStars had similar D_H values as measured by Ferguson analysis.

TEM imaging (Figure 1 e-i and Supporting Information Figure SI-4), was used to measure the size of the NStars. Increasing the HEPES/Au ratio on the geometry of the particles resulted in NStars with increasing arm lengths, while the core diameter remained mostly uniform (Supporting Information, Figure SI-5). Eccentricity, defined as the distance from the middle of the longest axis to the intersection of the two longest axes of the NStar, increased with increasing HEPES concentrations (Supporting Information, Figure SI-5).

Quantifying the extinction coefficient, ε

In order to quantify ε of the NStars, the extinction spectrum of each synthesis was first measured (Figure 2a). The SPR maximum redshifted with increasing HEPES concentration (Figure 2b). To quantify the amount of Au for a given NStar solution, the NStars were separated from unreacted Au and then dissolved in aqua regia. The concentration of Au ions, quantified by ICP-AES, ranged from 127-149 mg/l. Based on an original concentration of Au^{3+} of 158 mg/ml, 80-95% of the Au^{3+} ions were reduced in NStar formation. Therefore, the synthesis reaction yield is intermediate between NRs[16] (15%, in a seed-mediated synthesis approach) and spherical Au NPs (>95%, by citrate boiling)[16].

TEM images of NStars were used to calculate the volume of an individual NStar. An average of 6 arms in each NStar was determined by tilting the TEM stage ±30º. ImageJ was used to draw boundaries around the NStars to obtain the diameter of the maximum inscribed circle (cyan line and circle, Figure 2c); and the longest, middle and shortest arm lengths (red, green and blue lines, respectively, Figure 2c). Because TEM images show 2D projections of the NStars, which could adopt a variety of configurations on the TEM grid, the volume of the NStars was measured

if they were positioned in different configurations, obtaining a maximum difference in volume of 5% with different configurations. Therefore, NStars were modeled using the measured arm distances as the maximum lengths of the NStar arms, and the diameter of the maximum inscribed circle as the internal diameter of the NStars (Figure 2d). For each synthesis, at least 100 NStars were measured for statistical significance. The measured NStar dimensions were used to draw the 3D models of the NStars in AutoCAD (Figure 2d); AutoCAD's functions _MASSPROP and AREA were used to calculate the volume and area of individual NStars (Table 1).

Consequently, knowing the volume of individual NStars, the extinction spectrum of each NStar solution, and the total Au ion concentration in each solution, it was possible to determine ε_{expt} for each NStar sample (Table 1). ε_{expt} values at the SPR maximum ranged from 5.7 x 10^8 to 26.8 x 10^8 M^{-1} cm^{-1}. These values were on the same order of magnitude as measured values for NRs and NPs of similar volumes[16].

Simulating the extinction spectra by the discrete dipole approximation (DDA)

To gain further insight into the nature of the NStar ε, the extinction cross section of the NStars was simulated using the discrete dipole approximation (DDA) with the freely-available DDSCAT package. DDA approximates target particles of arbitrary geometries and complex refractive indexes, as an array of polarizable points located in a cubic lattice. We divided each NStar volume into at least 20000 dipoles, as suggested by other reports[23]. We averaged the extinction cross section between light interacting with the particle at the three major perpendicular axes by rotating the nanoparticle with respect to the incident light. This allowed calculation of the extinction (Q_{ext}), absorption (Q_{abs}) and scattering (Q_{scat}) cross-sections (Supporting information SI-6). We used Q_{ext} obtained from the simulations to calculate theoretical extinction coefficients (in units of M^{-1} cm^{-1}) of the NStars (ε_{theory}) using the formula[17]:

$$\varepsilon = {C_{ext}N_A}/{\ln 10} = N_A\left({10^{-17}}/{\ln 10}\right)\left({9\pi}/{16}\right)^{1/3} V^{2/3}Q_{ext}$$

where Q_{ext} is the maximum extinction cross-section of the NStars, V is the NStar volume and N_A is Avogadro's number. ε_{theory} values at the SPR maximum ranged from 7.8 x 10^8 to 35.3 x 10^8 M^{-1} cm^{-1} (Table 1).

The simulated extinction cross-sections spectra of the NStars (Figure 3) showed that SPR red-shifted with increasing arm length, analogous to the experimental results. Simulated spectra had narrower extinction full-width at half maximum (FWHM) compared to the experimentally measured spectra (Supporting Information, Figure SI-7), which has also been observed for nanospheres, NRs[17, 24, 25], and other metallic NPs[26], and can be explained by the fact that DDSCAT approximates an ideal and monodisperse particle shape that does not interact with other NPs in solution. Moreover, simulation results showed a SPR maximum red-shifted compared to the experimental values. This difference could be due to polydispersity of the NStar samples (Supporting Information Figure SI-8, cluster analysis and simulations of nanostars), where NStars with different eccentricities can be obtained during the synthesis, interactions leading to aggregation, slight truncations of the NStar edges[25], or a difference in the refractive index of the medium around the particles because of the capping BPS[27].

ε_{theory} exhibited a linear dependence on the SPR maximum (open squares, Figure 4a), as was observed for ε_{expt}. Moreover, we observed a linear dependence of ε_{theory} on $V^{2/3}$ (open squares, Figure 4b), which has been previously reported for NRs[28]. We observed that values for ε_{theory} tend to be lower than ε_{expt}, which has also been observed for NRs[29]. Also, we could observe that the SPR maximum was linearly dependent on the $V^{2/3}$ of the NStars (Figure 4c). Figure 4 shows

that the SPR maximum can be used to approximate the NStar ε_{expt} if the NStar dimensions or the plasmon absorbance data are available, and thus can be used to determine the NStar concentration in solution. The SPR maximum peak showed a linear correlation with the maximum arm length to core diameter (Supporting information, SI-9)[29].

NStar bioconjugation to DNA and proteins

Because NStars are attractive for biological applications, we covalently conjugated them to ssDNA aptamers[30] and also antibodies that recognize mouse immunoglobulin G. We used the ε_{expt} values obtained above to quantify the Ab and DNA coverage on the NStars. Both the antibodies and aptamers conjugated to the NStars were fluorescently tagged to enable quantification of their loading (See Methods). ssDNA thrombin binding aptamer (TBA) was conjugated to the NStars via covalent conjugation to a 5' thiol. TBA loadings on the NStar200, NStar350, NStar500 and NStar750 were $8.8 \pm 0.4 \times 10^{12}$, $11.6 \pm 0.5 \times 10^{12}$, $7.7 \pm 0.3 \times 10^{12}$ and $1.9 \pm 0.1 \times 10^{12}$ DNA molecules·cm^{-2}, respectively calculated from supernatant-loss measurements of unbound DNA. Loadings are similar in order of magnitude to published values observed for TBA on NRs[31] (a loading of 5.6×10^{12}-12.3×10^{12} for NRs with 1256 nm^2 area), and spherical NPs of similar surface areas[32] (loadings of 17×10^{12} for NPs with 1766 nm^2 area). Extinction spectra of NStar-DNA conjugates were slightly red-shifted relative to unconjugated NStars, but not significantly broadened, showing that they were stable in solution (Figure 5a-d), similar to NRs and nanospheres.[33 34] Ferguson analysis of gel electrophoresis showed that NStar D_H increased ~7 nm upon DNA conjugation (Figure 5e). This increase in D_H correlates with the secondary structure of the TBA, which is a folded 15mer with a 15mer spacer[35], suggesting that Ferguson analysis is accurate in quantifying NStar size after bioconjugation. However, DLS measurements showed a larger increase in D_H of 30-90 nm upon DNA conjugation (Figure 5h-k), which

suggests aggregation of the NStar-DNA in solution as opposed to in an electric field. This difference in D_H is somewhat expected given the different experimental conditions used to measure D_H for gel electrophoresis vs. DLS. Ferguson analysis showed a decrease in NStar ζ (Figure 5f) due to the negative charge of DNA. Conjugated gold NStars were retarded in gel electrophoresis relative to free NStars (Figure 5g), revealing that the bound DNA affected both NStar size and charge.

We also explored bioconjugation of NStars to fluorescently labeled antibodies (IgG) via covalent attachment (see Methods). IgG loading on the NStars were 3.0±0.6, 5.7±1.2, 31.3±1.5 and 3.3 ± 0.1 IgG molecules per NStar for NStar200, NStar350, NStar500 and NStar750 respectively, measured from supernatant-loss of unbound antibodies. Ab loadings were calculated assuming a 67.5 nm^2 top view footprint of an IgG antibody and were 3-10x lower than described for nanospheres.[36] The lower loading of Abs could be due to the irregular surfaces of the NStars, where curvature effects could potentially be undesirable for conjugation to the relatively large Abs[37]. Extinction spectra were not significantly broadened after bioconjugation, suggesting that NStars were stable in solution after Ab conjugation (Figure 5a-d). Ferguson analysis showed an increase in D_H of 7 nm upon conjugation (Figure 5e), which correlates well with the sizes and loadings of Abs on the NStars[38]. However, DLS showed a larger increase in average D_H (52 nm) (Figure 5h-k), which could be due to aggregation. Ferguson analysis showed that ζ of the NStars decreased upon antibody binding due to the negative charge of the Abs (Figure 5f). These results show that the NStars can be conjugated to DNA and proteins and that the ε_{expt} can be used to quantify biomolecule footprint on the NStar surfaces.

CONCLUSION

Au NStars are promising for a broad range of biological applications due to their strong and highly tunable extinction in the visible. One of the challenges in characterizing NStars is that their asymmetry and irregular shape complicate volume estimation, thereby presenting challenges for determining concentration. The molar extinction coefficient, ε_{expt}, of NStars can be used to measure their concentration, and it is a critical parameter when using NStars in biological applications. We have quantified the molar extinction coefficient ε_{expt} for NStars of different geometries and sizes, by correlating their extinction with the concentration of Au particles, which was measured by analyzing TEM images of the NStars, and counting Au ions by ICP-OES. The results correlate with DDSCAT computational models of the NStars. We use the experimental values of ε_{expt} to quantify NStar concentration, and to quantify biomolecule coverage measurements on NStar-Ab and NStar-DNA conjugates. DNA aptamers and antibodies were conjugated successfully to the Au nanostars. Nanostar curvature effects do not appear to hinder DNA conjugation to the NStars, but do seem to hinder conjugation to the relatively larger antibodies. Future work includes modification of NStar surface chemistry to increase the efficiency of antibody conjugation to NStars.

FIGURES

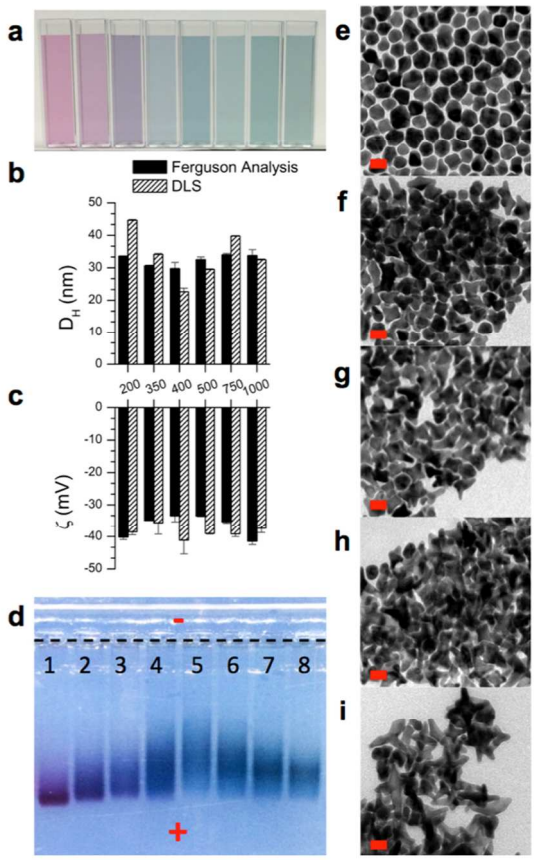

Figure 1. Gold NStars made with HEPES. a) Vials of NStars made with increasing HEPES (left to right), b) DLS, and c) zeta potential, d) agarose gel electrophoresis of NStars synthesized with increasing HEPES. Left to right: (1) NStar200, (2) NStar350, (3) NStar400, (4) NStar500, (5) NStar600, (6) NStar750, (7) NStar900, (8) NStar1000), e-i) TEM images of (e) NStar200, (f) NStar350, (g) NStar500, (h) NStar750, (i) NStar1000.

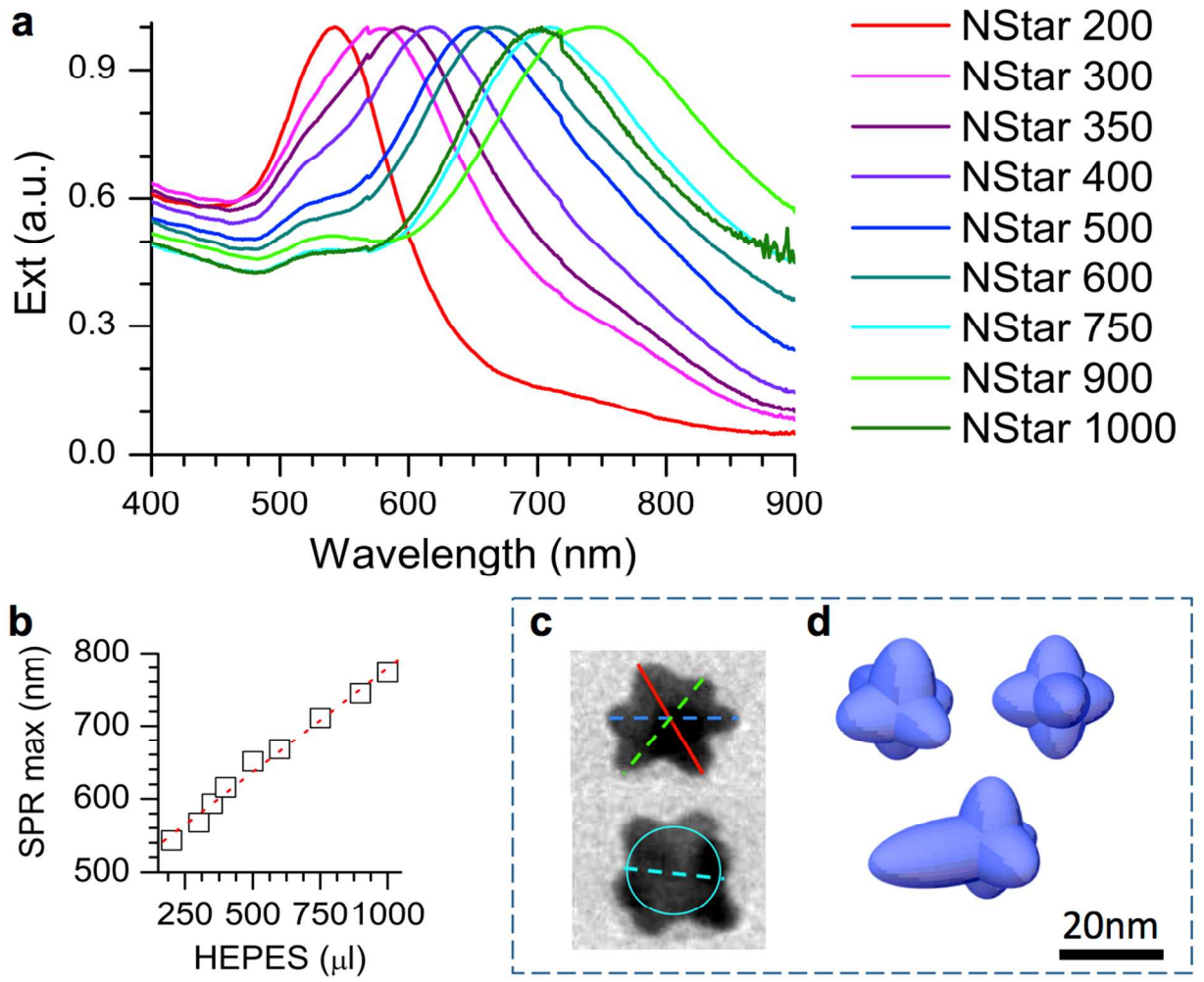

Figure 2. a) UV-vis extinction spectra of NStars synthesized with increasing HEPES concentration, b) SPR maximum wavelength as a function of the HEPES reaction concentration in the reaction, c) TEM images of individual NStars and schematic of how the geometric parameters of maximum arm length (red line), medium arm length (green dashed line), short arm length (blue dashed line), and internal diameter (cyan dashed line and circle) are extracted from the images, d) example of geometric model of a 6-arm NStar.

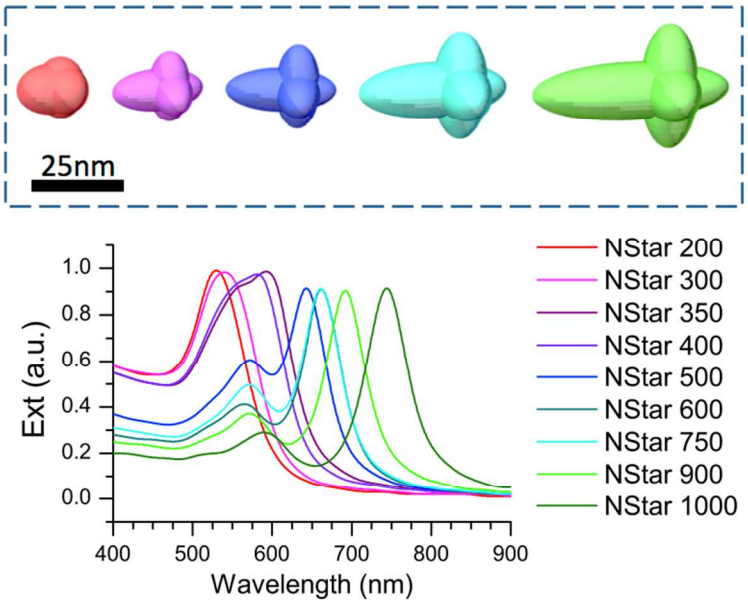

Figure 3. Simulated extinction spectra for NStars of different geometries measured by TEM imaging.

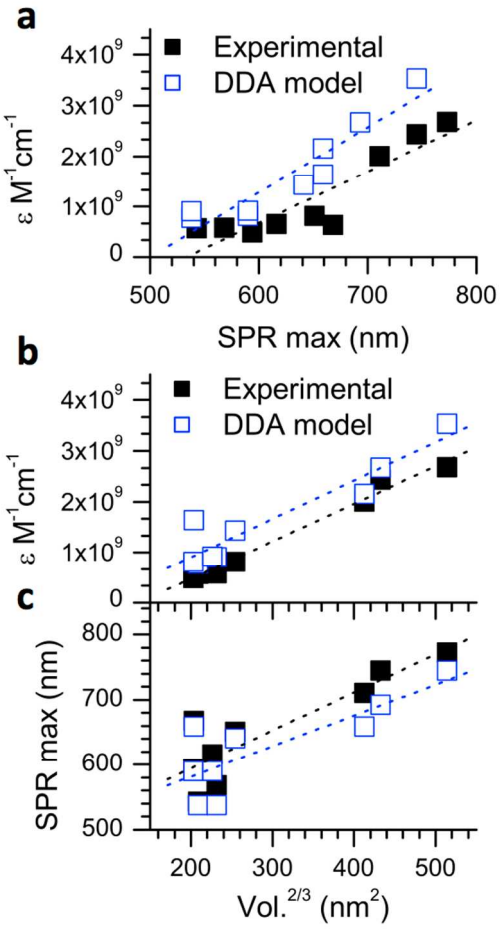

Figure 4. ε_{theory} (blue open squares) and ε_{expt} (black filled squares) as a function of a) SPR max and b) NStar volume $V^{2/3}$. c) SPR maximum as a function of volume, $V^{2/3}$. Linear dependence of the SPR with ε_{theory} has been observed.

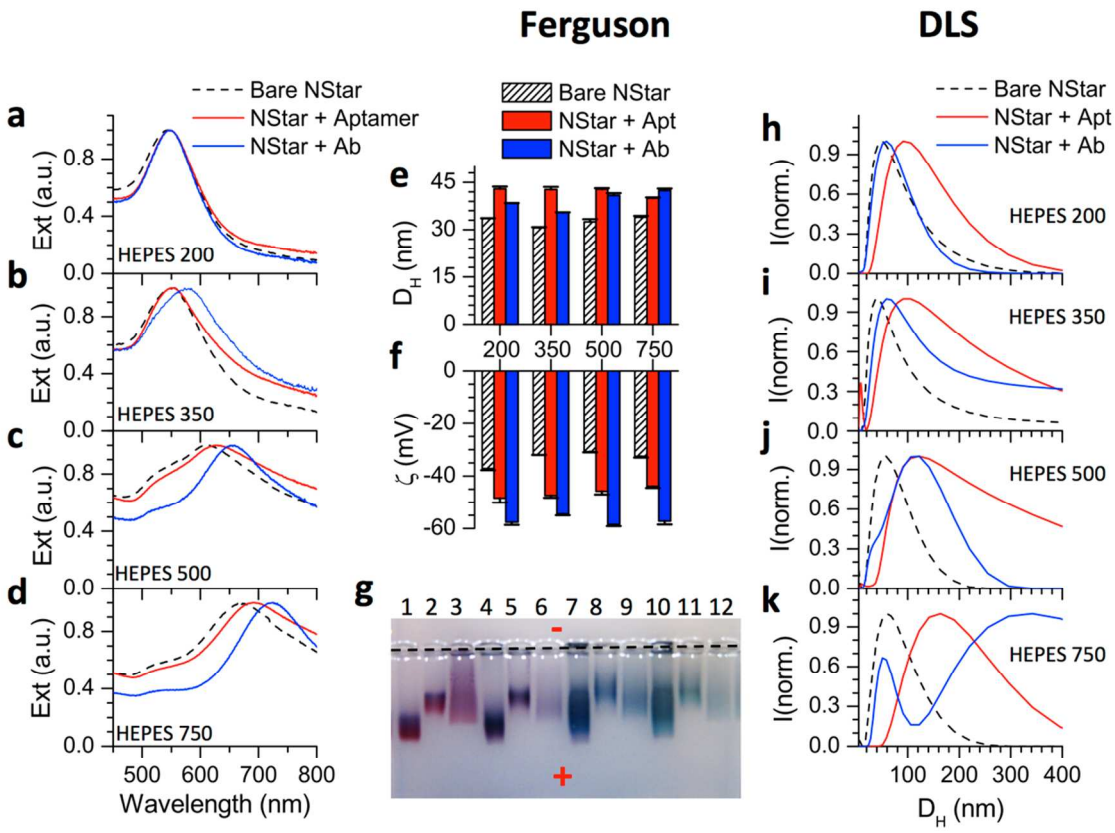

Figure 5. NStar bioconjugation to DNA and antibodies. Extinction spectra of a) NStar200, b) NStar350, c) NStar500, d) NStar750 conjugated to TBA DNA (red) and antibodies (blue) compared to bare NStars (black dotted). Measurements of the e) Hydrodynamic diameter (D_H) and f) zeta potential by Ferguson analysis, before and after conjugation with antibodies (blue) and TBA DNA (red) g) gel electrophoresis in 0.5 % agarose gels in 0.5X TBE buffer. Lanes: 1) NStar200, 2) NStar200-DNA, 3) NStar200-Ab, 4) NStar350, 5) NStar350-DNA, 6) NStar350-Ab, 7) NStar500, 8) NStar500-DNA, 9) NStar500-Ab, 10) NStar750, 11) NStar750-DNA, 12) NStar750-Ab. DLS spectra of h) NStar200, i) NStar350, j) NStar500, and k) NStar750, before conjugation (black dashed line), and after conjugation with TBA (red) and antibodies (blue).

TABLES

Synthesis	Geometric factors				Optical properties			
	TEM size (nm)		AutoCAD reconstruction		Experimental		Simulation results	
	Max Length	Diam. circle	Area (nm^2)	Volume (nm^3)	SPR max (nm)	ε ($M^{-1}cm^{-1}$)	SPR max (nm)	ε ($M^{-1}cm^{-1}$)
NStar 200	21±4	15±3	$1.0x10^3$	$3.0x10^3$	543	$5.7x10^8$	538	$7.8x10^8$
NStar 300	24±5	15±3	$1.2x10^3$	$3.5x10^3$	568	$5.8x10^8$	538	$9.1x10^8$
NStar 350	26±6	12±3	$1.1x10^3$	$2.9x10^3$	594	$4.9x10^8$	590	$8.1x10^8$
NStar 400	26±5	13±3	$1.2x10^3$	$3.4x10^3$	616	$6.6x10^8$	590	$9.2x10^8$
NStar 500	31±7	12±4	$1.5x10^3$	$4.1x10^3$	651	$8.1x10^8$	641	$14.3x10^8$
NStar 600	30±9	11±3	$1.2x10^3$	$2.9x10^3$	668	$6.4x10^8$	659	$16.4x10^8$
NStar 750	41±11	16±6	$2.4x10^3$	$8.4x10^3$	711	$20.1x10^8$	659	$21.6x10^8$
NStar 900	46±12	16±3	$2.6x10^3$	$9.0x10^3$	745	$24.4x10^8$	693	$26.7x10^8$
NStar 1000	55±16	16±5	$3.2x10^3$	$11.6x10^3$	773	$26.8x10^8$	745	$35.3x10^8$

Table 1. Molar extinction coefficient values (ε) obtained by experiments and theory, geometric model parameters, and surface areas.

AUTHOR INFORMATION

Corresponding Authors

*Kimberly Hamad-Schifferli, schiffer@mit.edu, Lee Gehrke, lgehrke@mit.edu

Present Addresses

†Current address: Merck & Co. Inc., 770 Sumneytown Pike, West Point, PA 19486.

‡Current address: MIT Lincoln Laboratory, Lexington MA 02420

Author Contributions

The manuscript was written through contributions of all authors. All authors have given approval to the final version of the manuscript.

Funding Sources

Funding was from NIH NIAID (AI100190). HdP was funded by MIT-SUTD IDC and a Rafael del Pino Fellowship.

ACKNOWLEDGMENTS

The authors would like to thank the CMSE at MIT for the use of their equipment facilities. Authors would like to thank Dr. Vlad Liberman for advice on the simulations, and Prof. Kim Vandiver and Prof. Sunho Park for fruitful discussions.

ASSOCIATED CONTENT

Supporting Information. DLS, zeta-potential measurements, TEM images, image analysis, simulations, and characterization of bioconjugates are available as Supporting Information. This material is available free of charge via the Internet at http://pubs.acs.org.

ABBREVIATIONS

NStar: nanostar; NP: nanoparticle; NR: nanorod.

REFERENCES

1. Xie, J.; Lee, J. Y.; Wang, D. I. C. Seedless, Surfactantless, High-Yield Synthesis of Branched Gold Nanocrystals in HEPES Buffer Solution. *Chem. Mater.* **2007**, *19*, 2823-2830.

2. Xie, J.; Zhang, Q.; Lee, J. Y.; Wang, D. I. C. The Synthesis of SERS-Active Gold Nanoflower Tags for in Vivo Applications. *ACS Nano* **2008**, *2*, 2473-2480.

3. Webb, J. A.; Erwin, W. R.; Zarick, H. F.; Aufrecht, J.; Manning, H. W.; Lang, M. J.; Pint, C. L.; Bardhan, R. Geometry-Dependent Plasmonic Tunability and Photothermal Characteristics of Multibranched Gold Nanoantennas. *J. Phys. Chem. C* **2014**, *118*, 3696-3707. Liu, X.-L.; Wang, J.-H.; Liang, S.; Yang, D.-J.; Nan, F.; Ding, S.-J.; Zhou, L.; Hao, Z.-H.; Wang, Q.-Q. Tuning Plasmon Resonance of Gold Nanostars for Enhancements of Nonlinear Optical Response and Raman Scattering. *J. Phys. Chem. C* **2014,** *118*, 9659-9664.

4. Wang, Y.; Black, K. C. L.; Luehmann, H.; Li, W.; Zhang, Y.; Cai, X.; Wan, D.; Liu, S.-Y.; Li, M.; Kim, P.; Li, Z.-Y.; Wang, L. V.; Liu, Y.; Xia, Y. Comparison Study of Gold Nanohexapods, Nanorods, and Nanocages for Photothermal Cancer Treatment. *ACS Nano* **2013**, *7*, 2068-2077.

5. Yuan, H.; Khoury, C. G.; Hwang, H.; Wilson, C. M.; Grant, G. A.; Vo-Dinh, T. Gold Nanostars: Surfactant-Free Synthesis, 3D Modelling, And Two-Photon Photoluminescence Imaging. *Nanotechnology* **2012**, *23*.

6. Barbosa, S.; Agrawal, A.; Rodriguez-Lorenzo, L.; Pastoriza-Santos, I.; Alvarez-Puebla, R. A.; Kornowski, A.; Weller, H.; Liz-Marzan, L. M. Tuning Size and Sensing Properties in Colloidal Gold Nanostars. *Langmuir* **2010**, *26*, 14943-14950.

7. Nehl, C. L.; Liao, H. W.; Hafner, J. H. Optical Properties of Star-Shaped Gold Nanoparticles. *Nano Lett.* **2006**, *6*, 683-688.

8. Vo-Dinh, T.; Liu, Y.; Fales, A. M.; Ngo, H.; Wang, H.-N.; Register, J. K.; Yuan, H.; Norton, S. J.; Griffin, G. D. SERS Nanosensors and Nanoreporters: Golden Opportunities in Biomedical Applications. *Wiley Interdisciplinary Reviews: Nanomedicine and Nanobiotechnology* **2015**, *7*, 17-33; Yuan, H.; Khoury, C. G.; Wilson, C. M.; Grant, G. A.; Bennett, A. J.; Vo-Dinh, T. In Vivo Particle Tracking and Photothermal Ablation Using Plasmon-Resonant Gold Nanostars. *Nanomed-Nanotechnol.* **2012**, *8*, 1355-1363.

9. Minati, L.; Benetti, F.; Chiappini, A.; Speranza, G. One-Step Synthesis of Star-Shaped Gold Nanoparticles. *Colloid. Surface A* **2014**, *441*, 623-628.

10. Dam, D. H. M.; Lee, J. H.; Sisco, P. N.; Co, D. T.; Zhang, M.; Wasielewski, M. R.; Odom, T. W. Direct Observation of Nanoparticle-Cancer Cell Nucleus Interactions. *ACS Nano*

2012, *6*, 3318-3326; Song, H.-M.; Wei, Q.; Ong, Q. K.; Wei, A. Plasmon-Resonant Nanoparticles and Nanostars with Magnetic Cores: Synthesis and Magnetomotive Imaging. *ACS Nano* **2010**, *4*, 5163-5173.

11. Dondapati, S. K.; Sau, T. K.; Hrelescu, C.; Klar, T. A.; Stefani, F. D.; Feldmann, J. Label-free Biosensing Based on Single Gold Nanostars as Plasmonic Transducers. *ACS Nano* **2010**, *4*, 6318-6322.

12. Su, Q.; Ma, X.; Dong, J.; Jiang, C.; Qian, W. A Reproducible SERS Substrate Based on Electrostatically Assisted APTES-Functionalized Surface-Assembly of Gold Nanostars. *ACS Appl. Mater. Interfaces* **2011**, *3*, 1873-1879.

13. Pallavicini, P.; Chirico, G.; Collini, M.; Dacarro, G.; Dona, A.; D'Alfonso, L.; Falqui, A.; Diaz-Fernandez, Y.; Freddi, S.; Garofalo, B.; Genovese, A.; Sironi, L.; Taglietti, A. Synthesis of Branched Au Nanoparticles with Tunable Near-Infrared LSPR Using a Zwitterionic Surfactant. *Chem. Commun.* **2011**, *47*, 1315-1317.

14. Near, R. D.; Hayden, S. C.; Hunter, R. E.; Thackston, D.; El-Sayed, M. A. Rapid and Efficient Prediction of Optical Extinction Coefficients for Gold Nanospheres and Gold Nanorods. *J. Phys. Chem. C* 2013, *117*, 23950-23955; Haiss, W.; Thanh, N. T. K.; Aveyard, J.; Fernig, D. G. Determination of Size and Concentration of Gold Nanoparticles from UVrom UVrom UVfr*Anal. Chem.* **2007**, *79*, 4215-4221.

15. Khoury, C. G.; Vo-Dinh, T. Gold Nanostars For Surface-Enhanced Raman Scattering: Synthesis, Characterization and Optimization. *J. Phys. Chem. C* **2008**, *112*, 18849-18859.

16. Orendorff, C. J.; Murphy, C. J. Quantitation of Metal Content in the Silver-Assisted Growth of Gold Nanorods. *J. Phys. Chem. B* **2006**, *110*, 3990-3994.

17. Ungureanu, C.; Rayavarapu, R. G.; Manohar, S.; van Leeuwen, T. G. Discrete Dipole Approximation Simulations of Gold Nanorod Optical Properties: Choice of Input Parameters and Comparison With Experiment. *J. Appl. Phys.* **2009**, *105*.

18. Park, S.; Hamad-Schifferli, K. Evaluation of Hydrodynamic Size and Zeta-Potential of Surface-Modified Au Nanoparticle-DNA Conjugates Via Ferguson Analysis. *J. Phys. Chem. C* **2008**, *112*, 7611-7616; Park, S.; Sinha, N.; Hamad-Schifferli, K. Effective Size and Zeta Potential of Nanorods by Ferguson Analysis. *Langmuir* **2010**, *26*, 13071-13075.

19. Draine, B. T.; Flatau, P. J. Discrete-Dipole Approximation for Scattering Calculations. *J. Opt Soc. Am. A.* **1994**, *11*, 1491-1499; Draine, B. T.; Flatau, P. J. User Guide to the Discrete Dipole Approximation Code DDSCAT 7.2. **2012**.

20. Johnson, P. B.; Christy, R. W. Optical Constants of Noble Metals. *Phys. Rev. B* **1972**, *6*, 4370-4379.

21. Kumar, S.; Aaron, J.; Sokolov, K. Directional Conjugation of Antibodies to Nanoparticles for Synthesis of Multiplexed Optical Contrast Agents with Both Delivery and Targeting Moieties. *Nat. Protoc.* **2008**, *3*, 314-320.

22. Habib, A.; Tabata, M.; Wu, Y. G. Formation of Gold Nanoparticles by Good's Buffers. *Bull. Chem. Soc. Jpn.* **2005**, *78*, 262-269.

23. Sosa, I. O.; Noguez, C.; Barrera, R. G. Optical Properties of Metal Nanoparticles with Arbitrary Shapes. *J. Phys. Chem. B* **2003**, *107*, 6269-6275.

24. Link, S.; El-Sayed, M. A.; Mohamed, M. B. Simulation of the Optical Absorption Spectra of Gold Nanorods as a Function of Their Aspect Ratio and the Effect of the Medium Dielectric Constant. *J. Phys. Chem. B* **2005**, *109*, 10531-10532.

25. Prescott, S. W.; Mulvaney, P. Gold Nanorod Extinction Spectra. *J. Appl. Phys.* **2006**, *99*.

26. Kelly, K. L.; Coronado, E.; Zhao, L. L.; Schatz, G. C. The Optical Properties of Metal Nanoparticles: The Influence of Size, Shape, and Dielectric Environment. *J. Phys. Chem. B* **2003**, *107*, 668-677.

27. Lee, K. S.; El-Sayed, M. A. Dependence of The Enhanced Optical Scattering Efficiency Relative to that of Absorption for Gold Metal Nanorods on Aspect Ratio, Size, End-Cap Shape, and Medium Refractive Index. *J. Phys. Chem. B* **2005**, *109*, 20331-20338.

28. Jain, P. K.; Lee, K. S.; El-Sayed, I. H.; El-Sayed, M. A. Calculated Absorption and Scattering Properties of Gold Nanoparticles of Different Size, Shape, and Composition:• Applications in Biological Imaging and Biomedicine. *J. Phys. Chem. B* **2006**, *110*, 7238-7248.

29. Myroshnychenko, V.; Rodriguez-Fernandez, J.; Pastoriza-Santos, I.; Funston, A. M.; Novo, C.; Mulvaney, P.; Liz-Marzan, L. M.; Garcia de Abajo, F. J. Modelling the Optical Response of Gold Nanoparticles. *Chem. Soc. Rev.* **2008**, *37*, 1792-1805; Hao, E.; Schatz, G. C.; Hupp, J. T. Synthesis and Optical Properties of Anisotropic Metal Nanoparticles. *J. Fluoresc.* **2004**, *14*, 331-341.

30. Dam, D. H. M.; Culver, K. S. B.; Odom, T. W. Grafting Aptamers onto Gold Nanostars Increases in Vitro Efficacy in a Wide Range of Cancer Cell Types. *Mol. Pharmaceutics* **2014**, *11*, 580-587.

31. de Puig, H.; Federici, S.; Baxamusa, S. H.; Bergese, P.; Hamad-Schifferli, K. Quantifying the Nanomachinery of the Nanoparticle-Biomolecule Interface. *Small* **2011**, *7*.

32. Hill, H. D.; Millstone, J. E.; Banholzer, M. J.; Mirkin, C. A. The Role Radius of Curvature Plays in Thiolated Oligonucleotide Loading on Gold Nanoparticles. *ACS Nano* **2009**, *3*, 418-424.

33. Aubin, M.-E.; Morales, D. G.; Hamad-Schifferli, K. Labeling Ribonuclease S with a 3 nm Au Nanoparticle by Two-Step Assembly. *Nano Lett.* **2005**, *5* (3), 519-522; Nusz, G. J.; Marinakos, S. M.; Curry, A. C.; Dahlin, A.; H A., F.; Wax, A.; Chilkoti, A. Label-Free Plasmonic Detection of Biomolecular Binding by a Single Gold Nanorod. *Anal. Chem.* **2008**, *80*, 984-989.

34. Wijaya, A.; Hamad-Schifferli, K. Ligand Customization and DNA Functionalization of Gold Nanorods via Round-Trip Phase Transfer Ligand Exchange. *Langmuir* **2008**, *24*, 9966-9969.

35. Macaya, R. F.; Schultze, P.; Smith, F. W.; Roe, J. A.; Feigon, J. Thrombin-Binding DNA Aptamer Forms a Unimolecular Quadruplex Structure in Solution. *Proc. Natl. Acad. Sci. U. S. A.* **1993**, *90*, 3745-3749.

36. Pease, L. F., III; Elliott, J. T.; Tsai, D.-H.; Zachariah, M. R.; Tarlov, M. J. Determination of Protein Aggregation With Differential Mobility Analysis: Application to IgG Antibody. *Biotechnol. Bioeng.* **2008**, *101*, 1214-1222; Boehm, M. K.; Woof, J. M.; Kerr, M. A.; Perkins, S. J. The Fab and Fc Fragments Of IgA1 Exhibit a Different Arrangement from that in IgG: A Study by X-Ray and Neutron Solution Scattering and Homology Modelling. *J. Mol. Biol.* **1999**, *286*, 1421-1447.

37. Cederquist, K. B.; Keating, C. D. Curvature Effects in DNA:Au Nanoparticle Conjugates. *ACS Nano* **2009**, *3*, 256-260.

38. Yen, C.-W.; de Puig, H.; Tam, J. O.; Gomez-Marquez, J.; Bosch, I.; Hamad-Schifferli, K.; Gehrke, L. Multicolored Silver Nanoparticles for Multiplexed Disease Diagnostics: Distinguishing Dengue, Yellow Fever, and Ebola Viruses. *Lab Chip* **2015**, *15*, 1638-41.

TOC figure

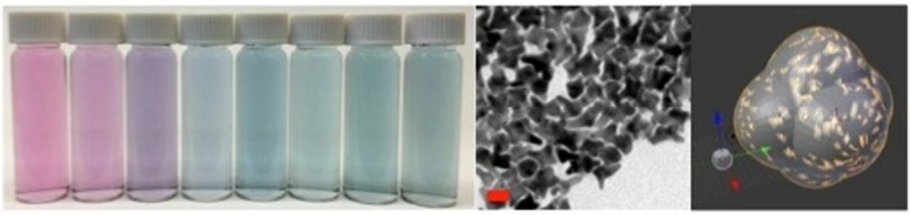

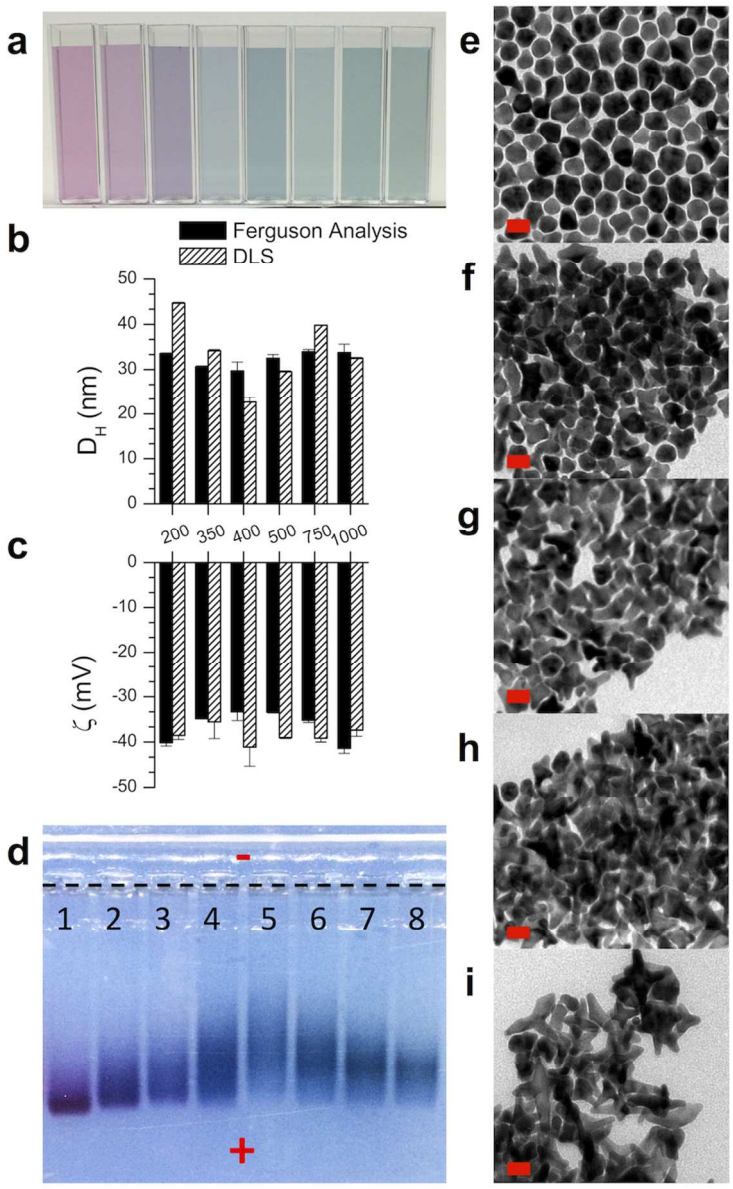

82x132mm (300 x 300 DPI)

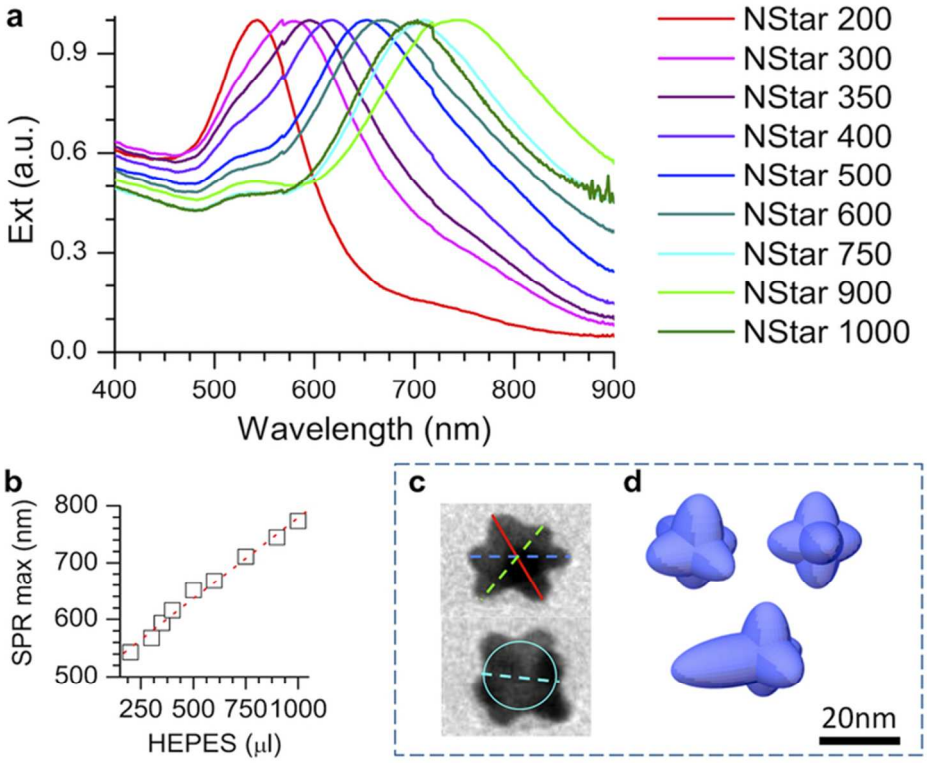

66x53mm (300 x 300 DPI)

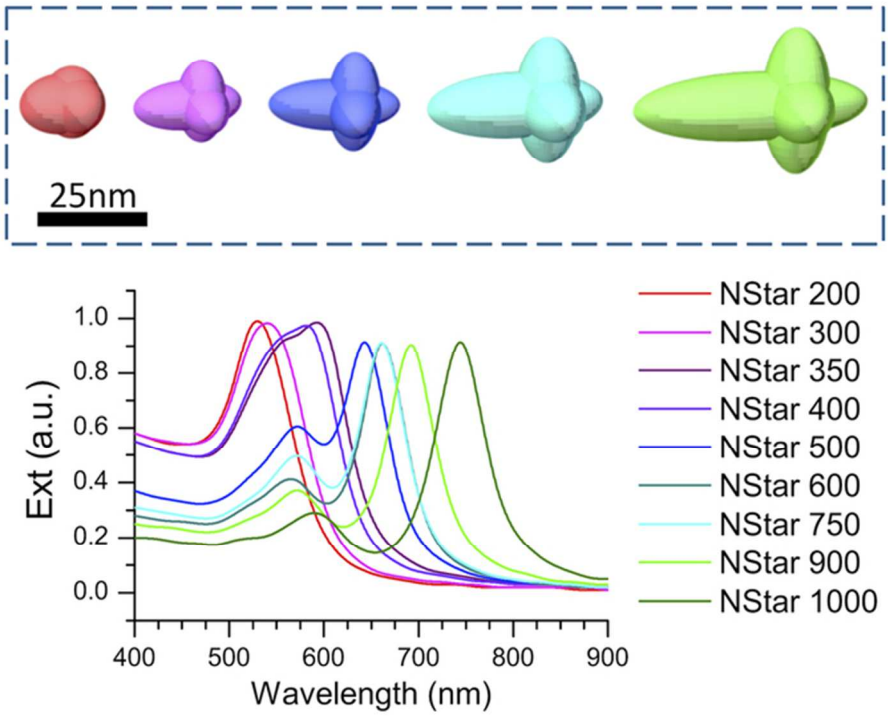

63x49mm (300 x 300 DPI)

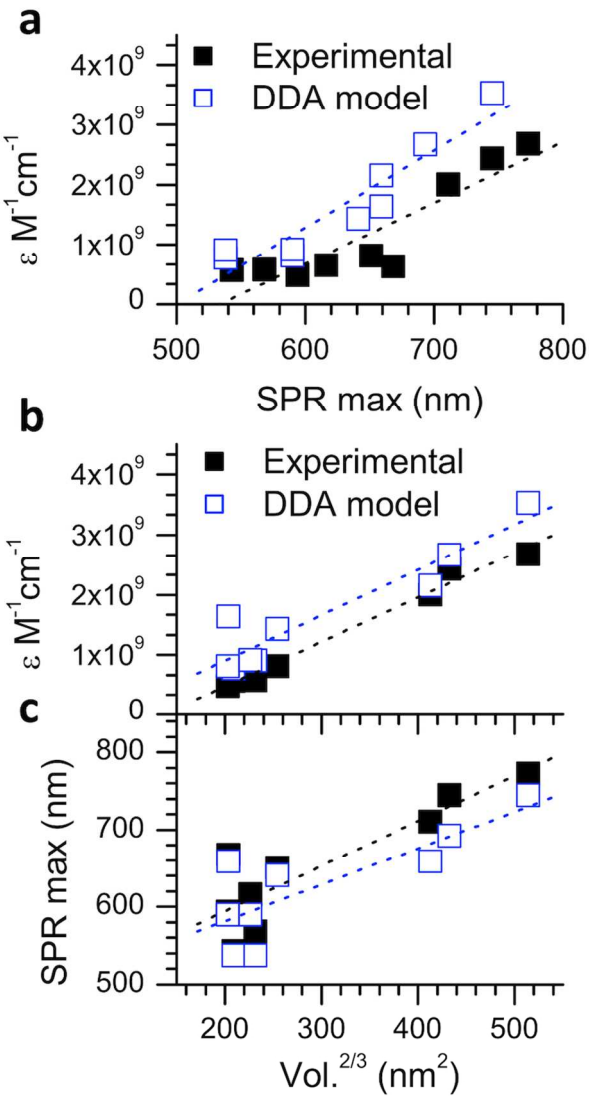

82x146mm (300 x 300 DPI)

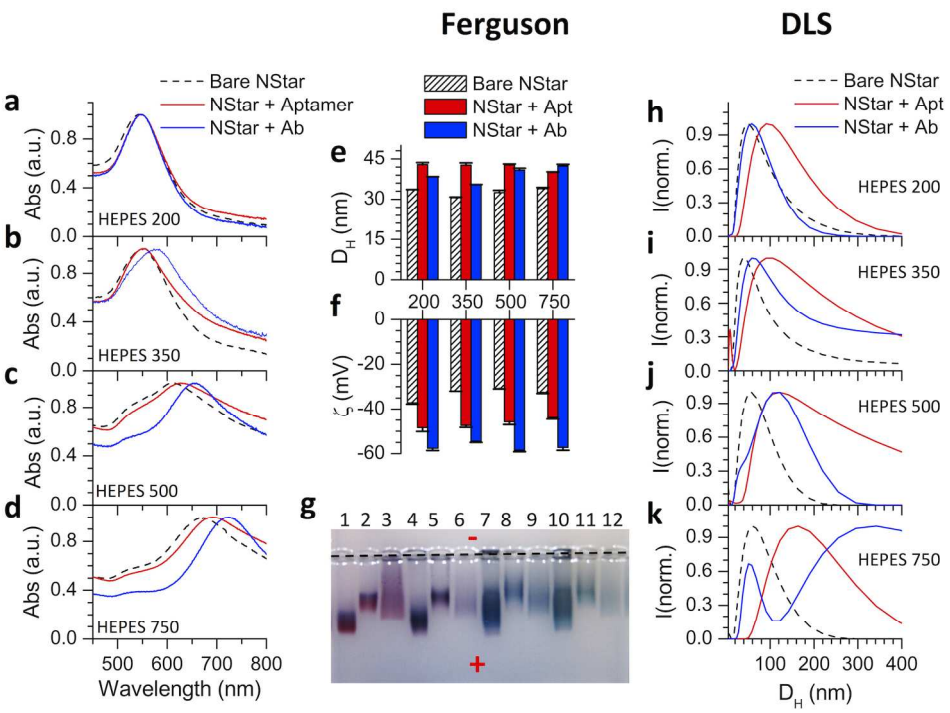

177x128mm (300 x 300 DPI)

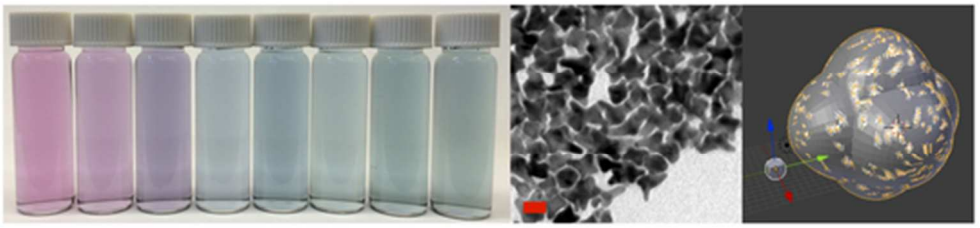

46x11mm (300 x 300 DPI)